

Article

Application of Activated Carbon Adsorbents Prepared from Prickly Pear Fruit Seeds and a Conductive Polymer Matrix to Remove Congo Red from Aqueous Solutions

Saadia Lahreche¹, Imane Moulefera^{2,3}, Abdelkader El Kebir⁴, Lilia Sabantina^{5,*} , M'hamed Kaid¹ and Abdelghani Benyoucef^{2,*} 

¹ Laboratory of Physico-Chemical Studies, University of Saïda, BP 138, Saida 20000, Algeria; lahrechmg2010@gmail.com (S.L.); kaid_wag@yahoo.com (M.K.)

² L.M.A.E. Laboratory, University Mustapha Stambouli of Mascara, Mascara 29000, Algeria; imanemoulefera@yahoo.fr

³ Department of Chemical Engineering, University of Malaga, Andalucía T.E.C.H, 29010 Malaga, Spain

⁴ Department of Electrical Engineering, University Mustapha Stambouli of Mascara, Mascara 29000, Algeria; a.elkebir@univ-mascara.dz

⁵ Junior Research Group "Nanomaterials", Faculty of Engineering and Mathematics, Bielefeld University of Applied Sciences, 33619 Bielefeld, Germany

* Correspondence: lilia.sabantina@fh-bielefeld.de (L.S.); a.benyoucef@univ-mascara.dz (A.B.)



Citation: Lahreche, S.; Moulefera, I.; El Kebir, A.; Sabantina, L.; Kaid, M.; Benyoucef, A. Application of Activated Carbon Adsorbents Prepared from Prickly Pear Fruit Seeds and a Conductive Polymer Matrix to Remove Congo Red from Aqueous Solutions. *Fibers* **2022**, *10*, 7. <https://doi.org/10.3390/fib10010007>

Academic Editor: Carlo Santulli

Received: 31 October 2021

Accepted: 7 January 2022

Published: 13 January 2022

Publisher's Note: MDPI stays neutral with regard to jurisdictional claims in published maps and institutional affiliations.



Copyright: © 2022 by the authors. Licensee MDPI, Basel, Switzerland. This article is an open access article distributed under the terms and conditions of the Creative Commons Attribution (CC BY) license (<https://creativecommons.org/licenses/by/4.0/>).

Abstract: The present work was aimed to evaluate the adsorption properties of activated carbons based on prickly pear seeds (PPS) and conductive polymer matrix based on polyaniline (PANI) for the removal of anionic Congo red (CR) dye from aqueous solutions. The adsorbent was prepared by polymerization of aniline in the presence of activated PPS by phosphoric acid and sodium hydroxide. The samples were characterized using X-ray diffraction (XRD), X-ray photoelectron spectroscopy (XPS), transmission electron microscopy (TEM), Fourier-transform infrared spectroscopy (FTIR), thermogravimetric analysis (TGA) and the Brunauer–Emmett–Teller (BET) methods. The adsorption kinetics were studied using UV-visible (UV/Vis) spectroscopy. The characterization data suggest that the adsorption of the Congo red dye is enhanced because PANI chain molecules, which are especially accountable for removal through π – π interaction and H-bonding with the CR, are adsorbed/tethered onto the acid-activated PPS (PPSH), and thus surmount the mass transfer limitation by being best exposed to the CR-adsorbed molecule. The adsorption kinetics follows the pseudo-second order process. The correlation coefficients (R^2) for Langmuir, Freundlich and Tempkin showed that the adsorption values obey Freundlich and Tempkin isotherm models. Moreover, the isotherm was most accurately described by the Freundlich model, and the maximum removal percentage was calculated to be 91.14% under optimized conditions of pH 6.6, 1 g/L of adsorbent dosage, and an initial CR dye concentration of 20 mg·L^{−1}. Importantly, the hybrid adsorbent exhibited the highest adsorption capacity (80.15%) after five cycles of the adsorption–desorption process. Thermodynamic parameters, such as entropy changes, enthalpy changes and Gibbs free energy, were also evaluated. These results indicated that the PANI matrix can generally be better utilized for the removal of Congo red dye when appropriately dispersed on the surface of suitable support materials. These results provide a new direction to promote the separable adsorbents with increasing performance for adsorption of dye impurities from wastewater.

Keywords: PANI; prickly pear seeds; activated carbon; adsorption; Congo red

1. Introduction

Dyeing effluents from textile finishing or printing industries pose a major environmental risk due to the pollution of freshwater with toxic and hazardous substances, which are dangerous to aquatic ecosystems and humans, as well as depleting drinking water

resources [1,2]. This problem is becoming more significant as the discharge of dyeing effluents has increased significantly in recent years [3]. For this reason, innovative, environmentally friendly, and renewable technologies for wastewater treatment are necessary, and the number of developments in this field is constantly increasing in recent years [4].

Congo red (CR) is a widely used anionic dye, which is widely used in research laboratories and industries and is an environmental problem [5,6]. Nowadays, various methods and technologies such as ozonization, degradation or oxidation, ion-exchange, membrane separation, biochemical processes, etc. are used to remove the dye from wastewater [7–10]. However, the above methods are relatively expensive and have low selectivity because they cannot be reused. Therefore, there is an urgent need for an effective method to remove dyes in a cost-effective, environmentally friendly, and selective manner.

Carbon based products (CBPs) are considered as perfect candidates for the removal of organic contaminants due to their elevated stability and high specific surface area [11,12]. Biomass-derived carbons offer many advantages over other carbons due to their stability and harmlessness as well as bio-based feedstocks [13–15]. However, the low porosity of the pyrolytic carbon formed means that biomass-derived carbons have a low specific surface area [16]. Consequently, selective, effective, and reversible adsorption and desorption of dyes with a CBP remains a major challenge. Biomass-derived porous carbons are produced using physical or chemical activation processes [17,18]. Bio-based precursors for activated carbon material such as fruits, seeds or leaves of plants, etc. are renewable raw materials and can contribute to the pollutants' elimination from wastewater [19–21]. In the study by Amran et al., adsorption properties of activated carbon prepared from Casuarina fruit were investigated for the removal of cationic (methylene blue) and anionic (Congo red) dyes [22]. Green synthesis of ZnO nanoparticles from Averrhoë carrambola fruit extract for Congo red dye photodegradation was investigated in the study by Chakraborty [23].

The prickly pear fruit (PPF) is the fruit of the prickly pear tree (*Opuntia ficus-barbarica*) and a member of the cactus family (*Cactaceae*), which grows in all semi-arid areas and is particularly cultivated in Central America and the Mediterranean region [24]. The utilization of this material could be a favorable alternative for the elimination of pollutants in wastewater due to its low cost, relative abundance, environmental friendliness, and effectiveness. The PPF is an oval fruit weighing from 70–220 g, containing a thick shell (30–60%), which consists of numerous hard-coated seeds (3–10%) [25]. PPF can be classified as an aliment of nutraceutical and functional significance because of its elevated content of chemical components that have beneficial feeding and health properties [26]. It is generally consumed as fresh fruit or prepared as compounds such as jam, juice, congealed fruit, and others [27]. After processing, the seeds are usually discarded because they contain high levels of unsaturated oil [28], which can be extracted by cold pressing. Recently, various research assessed the possibility of dried PPF material for pollutants' elimination from wastewater. Barka et al. [29] reported PPF adsorption efficiency of heavy metals (Cd and Pb) and dyes (Alizarin S, Eriochrome Black T and Methylene Blue) from aqueous solutions. Cid et al. [30] utilized PPF waste in its untreated and activated forms as adsorbent for dyes.

Among the conductive polymer, PANI is one of the most popular ones because it exhibits high redox stability, simple synthesis, and high performance capacity and is ecofriendly and inexpensive [31–33]. From the scientific and technological point of view, PANI is selected as an active material because of its easy preparation, efficiency, and broad effectiveness [33]. It has been shown that PANI is very well used in combination with hybrid materials to improve the properties, such as PANI/Cellulose [34], PANI/Walnut shell [35], PANI@Almond shell [36], PANI/Chitosan [37], and PANI modified almond [38].

In this study, polyaniline@activated-prickly-pear seeds (PANI@PPSH) were synthesized by simple in situ oxidative polymerization and characterized by various methods, including FT-IR, XPS, TEM, XRD, TGA, and BET. The prepared PANI@PPSH biocomposite was used for the elimination of Congo red (CR) dye from aqueous solutions. The influences of physicochemical parameters such as CR concentration, pH influence, and contact time on removal efficiency were studied. The modelling of kinetics and equilibrium isotherm for

CR removal by PPSH, PPSOH, and PANI@PPSH was determined. The renewal capability of PANI@PPSH bioadsorbent was also investigated.

2. Materials and Methods

2.1. Materials

The seeds of prickly pear (*Opuntia ficus-barbarica* A. Berger) fruits were collected from a plantation in the region of Mascara of western Algeria in August 2021. The monomer aniline (ANI) ($\geq 99.5\%$ purity, Aldrich, St. Louis, MI, USA), ammonium persulfate (APS) ($\geq 98\%$ purity, Merck KGaA, Darmstadt, Germany), ammonia solution (NH_4OH) (25% purity, Merck KGaA, Darmstadt, Germany), phosphoric acid (H_3PO_4) (70% purity, Merck KGaA, Darmstadt, Germany), sodium hydroxide (NaOH) (37% purity, Merck KGaA, Darmstadt, Germany), Congo red dye (CR) (dye content $\geq 35\%$, Sigma-Aldrich, St. Louis, MI, USA), ethanol ($\text{C}_2\text{H}_5\text{OH}$) (96% purity, Merck KGaA, Darmstadt, Germany), filter paper (EAPI Company, Annaba, Algeria) and the ultrapure H_2O (18.2 M Ω .cm, ELGA LabWater, Lane End, UK) were applied in all experiments.

2.2. Measurements

X-ray photoelectron spectroscopy (XPS) was applied to calculate the surface components of materials by a spectrometer (VG Microtech Ltd., London, UK). Wide-angle X-ray diffraction (XRD) patterns were performed at room temperatures with specimens on a Madison instrument (WI, USA) diffractometer with $\text{Cu}/\text{K}\alpha$ radiation ($\lambda = 1.5418\text{\AA}$) at a scanning rate of $0.02^\circ \text{min}^{-1}$ over a range of $2\theta = 0.2\text{--}60^\circ$. Fourier transform infrared spectrum (FT-IR) (Varian, Inc., Palo Alto, CA, USA) was implemented by a Bruker Inc. (Billerica, MA, USA) Model-Alpha spectrometer between $500\text{--}2000\text{ cm}^{-1}$. The morphologies of the samples were determined with a scanning electron microscope (SEM) Hitachi, S-4160, Iidacho, Japan). UV-Visible spectroscopy (Hitachi U3000-Spectrophotometer) was applied to calculate CR concentrations. Thermogravimetric analysis (TGA) was performed using a simultaneous thermogravimetric analyzer (Hitachi-STA 7200, Fukuoka, Ja-pan). The pH value was determined by an instrument (Multiparameter Benchtop Water Quality Meter, 86505-EB-AZ, Barcelona, Spain). Information about the BET surface area and porosimetry was provided using an Autosorb (iQ, Shanghai, China) system at liquid nitrogen temperature (77 K) [29,39].

The zero point of charge (pH_{PZC}) was determined according to the method described by Cid et al. [30]. First, the initial pH of the solution was studied in an array of 2.0–12.0 using HCl and NaOH in NaNO_3 solutions. After precise measurement of the $\text{pH}_{\text{initial}}$, an adsorbent was added to each flask and the solution was agitated for 48 h to reach the equilibrium. After this period, the pH of the solution (pH_f) was measured. The pH_{PZC} was derived from the curve $\text{pH} = \text{pH}_i - \text{pH}_f = f(\text{pH}_i)$ as the intercept of the abscissa.

2.3. Adsorbents' Preparation

2.3.1. Carbon Preparation

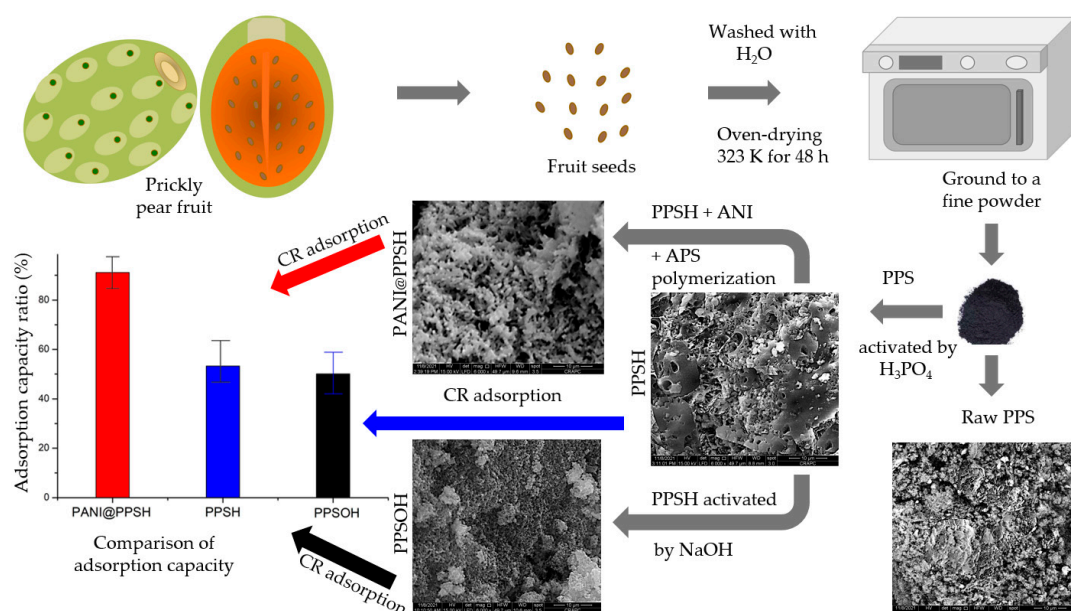
The PPS seeds were repeatedly washed with H_2O to remove foreign material and then oven dried at 323 K for 48 h. After these procedures, the PPS were ground to a fine powder in the size range of 30 to 70 μm using a laboratory mill (Fisher Bioblock Scientific, Illkirch, France).

Chemical activation was performed by blending the PPS (10 g) and H_3PO_4 (weight ratio 1:1). The suspension was then stirred for about 180 min until homogenized. Then, the solution was filtered and washed with deionized H_2O until the pH of the water became neutral [40]. Afterwards, the carbonization process of materials was carried out; the PPS- H_3PO_4 was converted into solid carbon (PPSH). The carbonization occurred by storing 20 g of PPS- H_3PO_4 at 110°C for 24 h. The impregnated samples were pyrolyzed in a furnace (Model DHG-9023A, Everich, Hangzhou, China) under an inert atmosphere at 450°C for 2 h. The PPSH sample was crushed with a mortar and sieved with a sieve, and the product was stored in plastic clamps and glass bottles. Similarly, the PPSH sample was treated and

activated with an aqueous NaOH solution at a concentration of 1 M. Then, the chemically treated samples were dried in an electric oven (Elba EEO-A4218, Fiamma Holdings Berhad, Bandar Manjalara, Malaysia) at 450 °C for 2 h, ground, and stored in plastic containers. This final product was named PPSOH.

2.3.2. PANI@PPSH Preparation

The chemical preparation of polyaniline with PPSH (PANI@PPSH) as nanoadsorbent was carried out according to the methodology proposed by Mahi et al. [30]. Dispersions of 1 g PPSH in 100 mL of H₃PO₄ (1 M) solution were performed by ultrasonic combustion for 30 min. Then, 1 mL of aniline (ANI) was added to the solution and the blend was sonicated for 1 h. Afterwards, 50 mL of H₃PO₄ acid (1 M) consisting of ammonium persulfate (APS) (oxidant: monomer molar ratio was 1:1) was added dropwise to the solution with continuous stirring and stirred overnight at room temperature. The product precipitate was filtrated and washed several times with C₂H₅OH and H₂O to eliminate excess oligomers containing the oxidant. Finally, the final PANI@PPSH adsorbent was dried at 70 °C for 24 h. A graphical exemplification of the preparation of the adsorbents is presented in Scheme 1.



Scheme 1. A graphical representation of the adsorbents prepared.

2.4. Adsorption Experiments

Batch adsorption experiments were conducted in 100 mL glass vials. In typical experiments, 0.1 g of adsorbent was added into the 100 mL CR solution (5, 10, 20, 30, 50, 100 and 150 mg L⁻¹, respectively) and shaken. After reaching equilibrium by shaking, the final CR concentration was filtrated and analyzed by UV-Vis. The removal percentage of CR was determined using the following equation [41]

$$\text{Removal} = \frac{(C_0 - C_{\text{eq}})}{C_0} \times 100\% \quad (1)$$

where C_0 is the initial CR concentration and C_{eq} is the equilibrium concentration of CR. The removal percentage was measured by varying the adsorbent quantity, initial concentration of CR, temperature and contact time. To determine the adsorption capacity, the uptake of CR per gram of adsorbent was determined using the following equation.

$$Q_{\text{eq}} = \frac{(C_0 - C_{\text{eq}})V}{m} \quad (2)$$

where Q_{eq} ($\text{mg}\cdot\text{g}^{-1}$) is the adsorption capacity at equilibrium, V (L) is the total volume of reaction solution, and m (g) is the mass of adsorbent.

3. Results and Discussion

3.1. Characterization and Structural Analyses

Figure 1a shows the XRD patterns of PANI, PPSH, PPSOH, and PANI@PPSH samples. The X-ray patterns of two materials (PPSH and PPSOH) showed the presence of a typical PPF structure. It had strong crystalline peaks at 16.89° and 23.49° , corresponding to the (110) and (002) planes of crystals [42]. Moreover, PANI was semi-crystalline in nature, as shown by three peaks centered at $2\theta = 16.45^\circ$ (011), 20.22° (020), and 25.87° (200), which was due to the presence of benzenoid with the quinonoid group in the polymer chain [43]. The characteristic peaks of two constituents were observed in the XRD patterns of PANI@PPSH, indicating that the hybrid material was successfully synthesized.

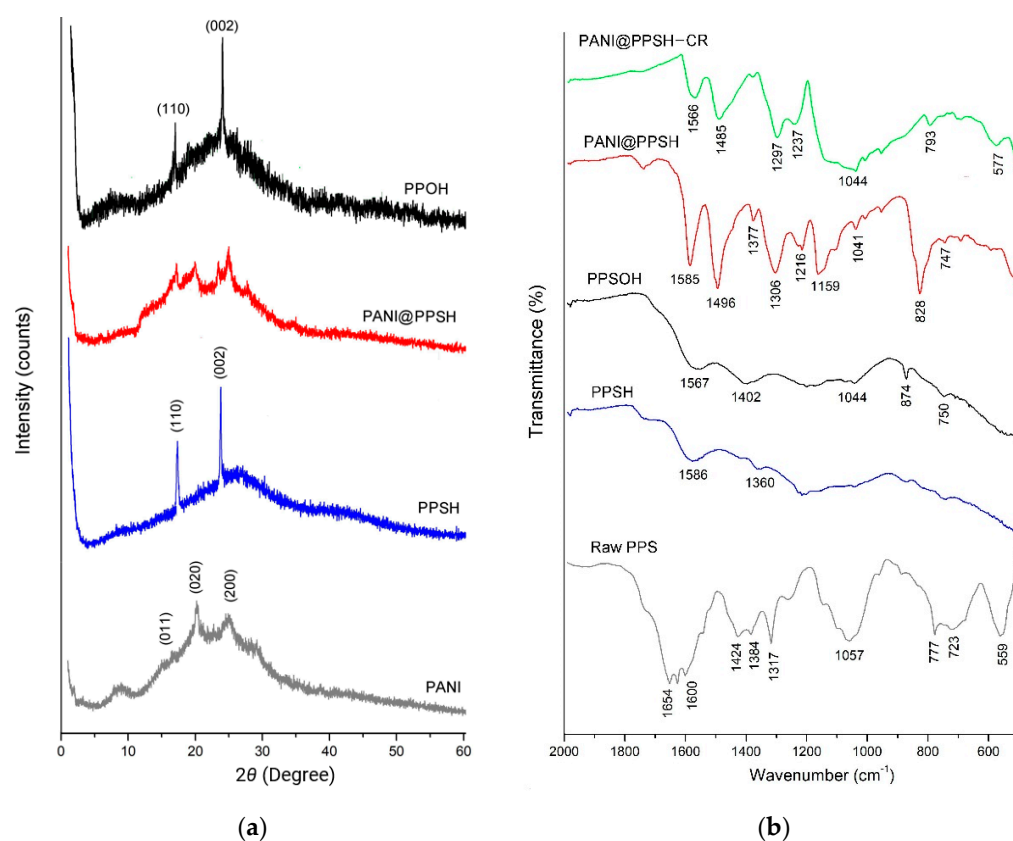


Figure 1. (a) X-ray diffraction (XRD) patterns and (b) Fourier-transform infrared spectroscopy (FT-IR) spectrum (before and after adsorption) of samples.

The raw PPS, PPSH, PPSOH, and PANI@PPSH (before adsorption) IR spectrum (Figure 1b) displayed that there were modifications in the surface sample. The activation by H_3PO_4 and NaOH led to a peptization and dissolution of polysaccharide, lignin, cellulose, and hemicellulose in the raw product [14]. The band at about $1600\text{--}1654\text{ cm}^{-1}$ can be assigned to the benzene ring ($\text{C}=\text{C}$). The disappearance of this band after chemical activation of PPS proved that the chemical bonds were broken during the carbonization process. Moreover, in the hybrid adsorbent, typical bands of PANI were found at 828 cm^{-1} due to $\text{C}-\text{C}$ stretching of quinoid rings and deformation of the benzenoid rings, respectively. The band at 1159 cm^{-1} for PANI appeared to be due to $\text{C}=\text{N}$ stretching vibration. The transmittance peak at 1306 cm^{-1} due to the $\text{C}-\text{N}$ bond, 1496 cm^{-1} due to the $\text{C}=\text{C}$ stretching vibration of benzenoid rings, and 1585 cm^{-1} due to the stretching vibration of quinoid rings and the observed peak positions are in agreement with the report of other work [33]. In addition, the IR spectrum was obtained for PANI@PPSH after CR adsorption. Based on the

shift of the spectra and the reduction and disappearance of the bands, it was determined CR adsorption by different functional groups had an influence.

The pore size distribution and also the surface area of adsorbents were studied using the Brunauer–Emmett–Teller (BET) theory (Figure 2a). All adsorbents exhibited type III isotherms and similar H3 hysteresis loop. The calculated BET surface areas of PPSH, PANI, PPSOH, and PANI@PPSH were $42.79 \text{ m}^2 \cdot \text{g}^{-1}$, $29.25 \text{ m}^2 \cdot \text{g}^{-1}$, $20.21 \text{ m}^2 \cdot \text{g}^{-1}$, and $51.28 \text{ m}^2 \cdot \text{g}^{-1}$, respectively. The total average pore size and BET area of the adsorbents are presented in Table 1. The larger pore size and pore volume of the PANI@PPSH composite compared to the other adsorbents might be credited to the formation of new mesopores at the interface between the PANI layers and the PPSH, resulting in more active sites. The increased pore volume and pore size of the hybrid adsorbent would be a beneficial feature to promote the migration of adsorbate molecules into the mesopores during the adsorption process [44].

Table 1. Textural properties of adsorbents.

Materials	S_{BET} ($\text{m}^2 \cdot \text{g}^{-1}$)	Pore Volume ($\text{cm}^3 \cdot \text{g}^{-1}$)	Average Pore Size (nm)	pH_{PZC}
PANI	42.79	1.81	28.52	5.1
PPSH	29.25	2.34	36.77	6.9
PPSOH	20.21	2.21	37.55	9.2
PANI@PPSH	51.28	2.85	40.94	6.7

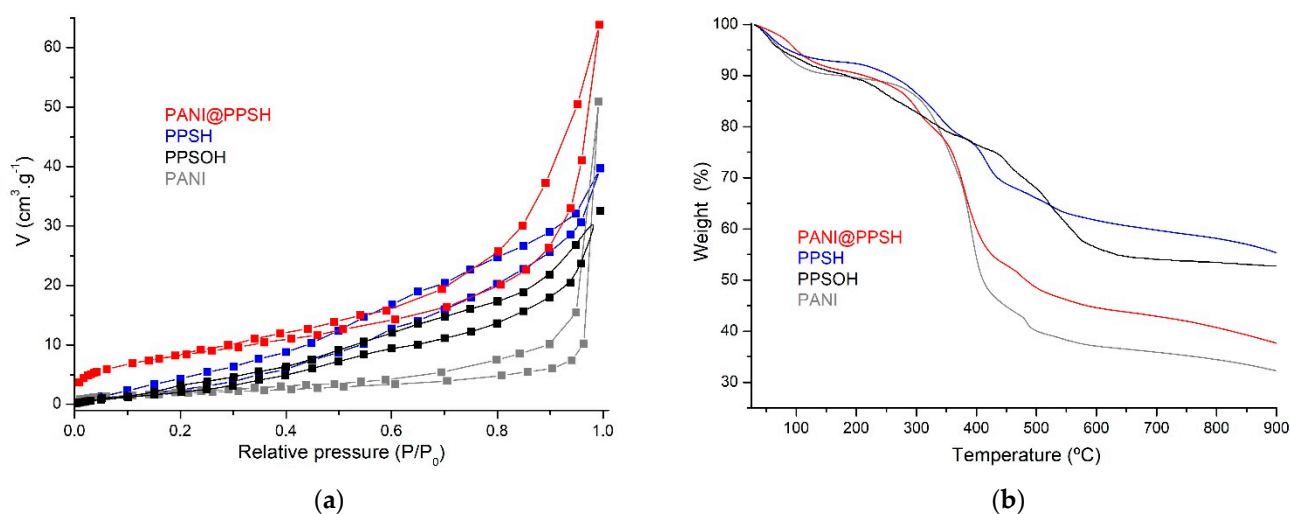


Figure 2. (a) Brunauer–Emmett–Teller (BET) surface area and (b) thermogravimetric analysis (TGA) of samples.

The values of the pH_{PZC} are shown in Table 1. These indicate that the PANI and PPSOH adsorbents had a contrary effect on the surface of the adsorbents. On the other hand, the PPSH and PANI@PPSH materials exhibited a slightly acid surface (pH_{PZC} is 6.9 and 6.7, respectively). The PPSOH adsorbent had a basic character (pH_{PZC} is 9.2), and PANI had an acid character (pH_{PZC} is 5.1). In contrast, the two adsorbents (PPSH and PANI@PPSH) exhibited $\text{pH}_{\text{PZC}} < 7$, indicating an acid character of their surfaces.

TGA was used for the evaluation of the thermal stability of different adsorbents and also for the evaluation of the decomposition behavior of the prepared materials (Figure 2b). The weight loss (TGA) of PANI@PPSH consisted of the drying water loss stage (25–190 °C) with the weight loss (9.54 mass%). During the second stage, the weight loss (43.67 mass%) in the range from 190 °C to 530 °C was assigned to the breaking of chemical compounds of PANI from their frameworks. Finally, the carbonization stage (≥ 530 °C) showed a weight loss of 8.96% at 900 °C, while PANI amounted to 69.21%. This was because the presence of PPSH on the polymer chain favored the growth of the crystal [38], while the PPSH

and PPSOH adsorbents showed an overall weight losses at 900 °C of 44.34% and 46.92%, respectively.

To detect the molecular structure of PANI@PPSH, XPS analysis was carried out, as depicted in Figure 3. The C1s spectra (Figure 3a,b) of PPSH and PANI@PPSH were resolved into four types of C atoms, which were attributed to C–C/C=C bonds (peak at 284.5 eV) and to oxygen-containing bonds such as C–O (285.5 eV), C=O (287.3 eV), and O–C=O (289.0 eV) [45]. PPSH had the highest oxygen content among the two adsorbents. Moreover, two peaks appeared in the N1s spectrum of PPSH (Figure 3c). The first peak at 399.46 eV was associated to the –NH₂, which belonged to the characteristic basic functional group of seeds fruit. Another peak at 401.41 eV was assigned to –NH–C=O (amide) of the acetylated unit. In comparison with PANI@PPSH, three peaks at 398.27 eV, 400.46 eV, and 401.87 eV were evident, demonstrating the presence of –N=, –NH/–NH–C=O, and –NH⁺ groups [46], as shown in Figure 3d. Two peaks appeared in the N1s spectrum of PPSH (Figure 4c). The first peak at 399.46 eV was associated to the –NH₂, which belonged to the characteristic basic functional group of the seeds fruit. Another peak at 401.41 eV corresponded to the –NH–C=O (amide) of the acetylated unit. In comparison with PANI@PPSH, three peaks at 398.27 eV, 400.46 eV, and 401.87 eV were evident, demonstrating the presence of –N=, –NH/–NH–C=O, and –NH⁺ groups [46], as shown in Figure 3d. The XPS analysis further proved the successful synthesis of the hybrid adsorbent.

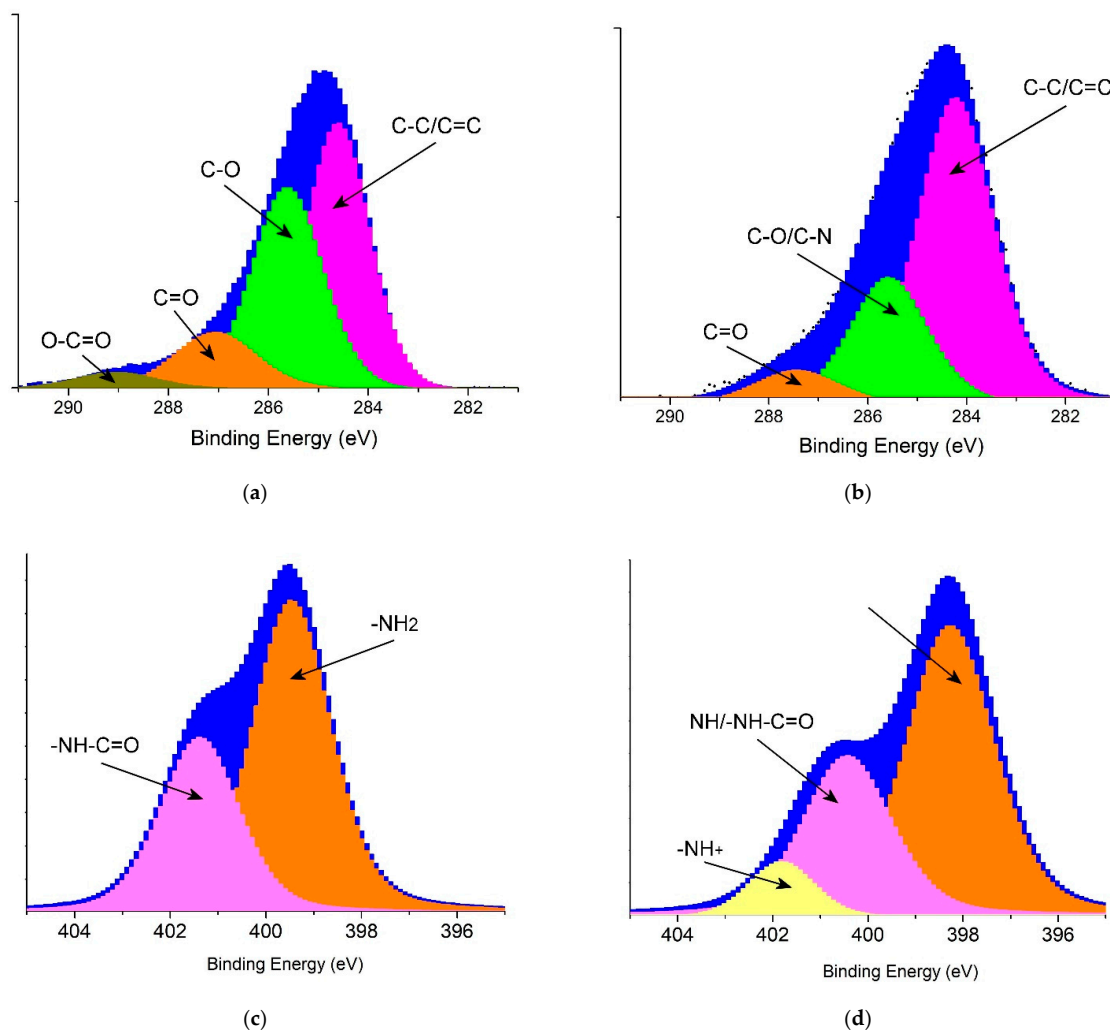


Figure 3. X-ray photoelectron spectroscopy spectra of adsorbents: (a) C1s of PPSH, (b) C1s of PANI@PPSH, (c) N1s of PPSH and (d) N1s of PANI@PPSH.

Figure 4 shows the surface morphology of the synthesized adsorbents. The SEM micrographs showed remarkable change in the surface morphology of PPS after activation. As shown in Figure 4a, the PPS surface was very dense, without pores and cavities. However, it is clear from Figure 4b,c that activation by acid or base caused a surface modification of PPS, leading to a rough and partly porous surface. Subsequently, the reaction of the PANI chain in the existence of PPSH resulted in a highly porous surface (Figure 4d); the higher pore transformation of PPSH led to better interaction with the polymer matrix and PPSH, resulting in the formation of significant spaces and pores on the surface.

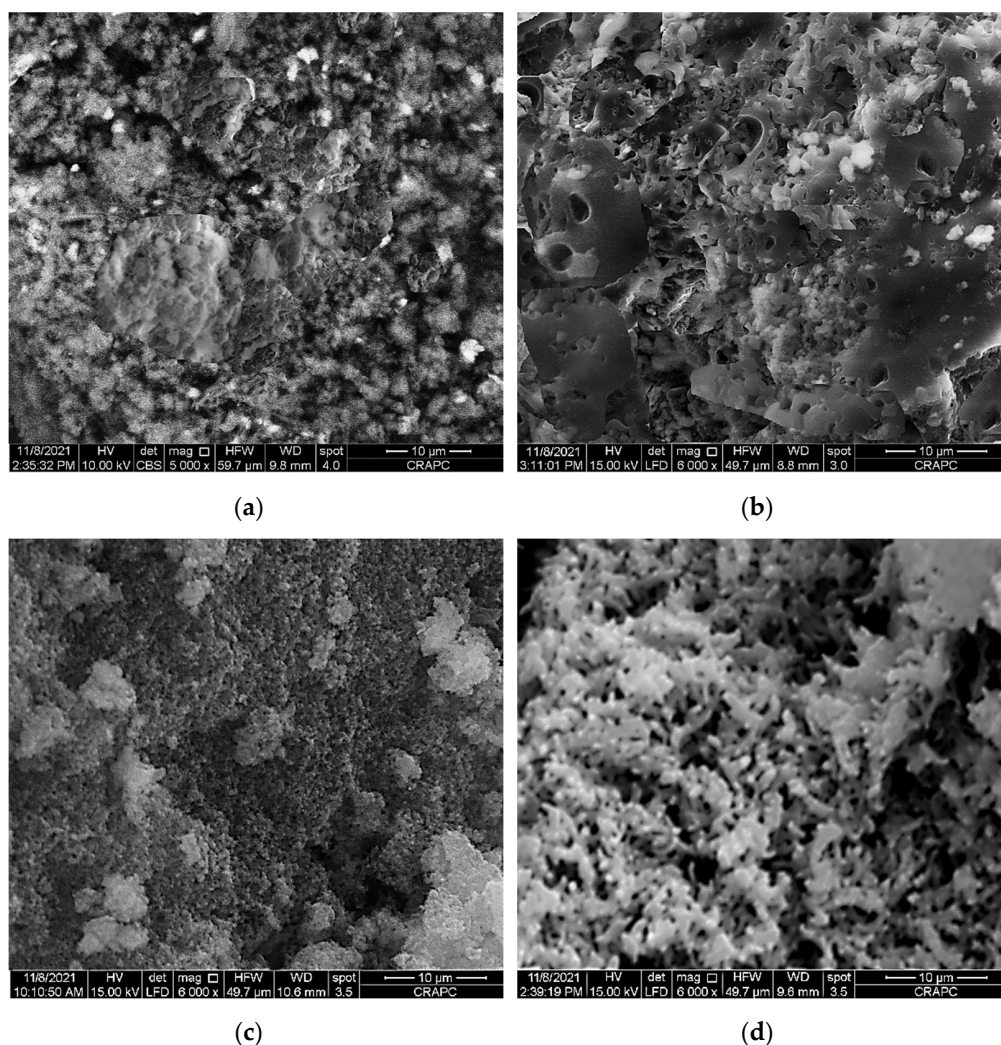


Figure 4. Scanning electron microscope (SEM) micrographs of: (a) raw PPS, (b) PPSH, (c) PPSOH and (d) PANI@PPSH.

3.2. Adsorption Assessments

3.2.1. Influence of pH

The pH is one of the most important factors affecting the surface charge and determining the elimination efficiency of the adsorbent, as the pH affects several parameters in the removal process, including the distribution of organic ions, the surface charges of the adsorbents, and dissociation ratio of the functional groups located on the active surface sites of the adsorbent. Interestingly, the pH value showed distinct behavior for both ionic and cationic dyes. In the case of cationic dyes, the percentage of organic pollutant elimination decreased at low pH, which was due to the excess of H^+ ions competing with the organic pollutant structure for the active surface sites. In contrast, for ionic dye, the adsorbent adsorbed negatively charged ionic dye at the low pH, corresponding to the positively

charged surface [47]. Congo red is an ionic organic pollutant that is utilized as an acid/base detector. While the pH of Congo red (CR) solution is less than pH 4.71, its color converts to dark blue [48]. The removal process was investigated under different pH solutions in the pH range from 2 to 12. The impact of the pH solution on the ratio of the adsorbed CR dye is shown in Figure 5a. It can be seen that the removal capacity of the PANI@PPSH hybrid adsorbent for CR increased when the pH was raised to 6.5. The subsequent increase in pH resulted in a decrease in the removal capacity of the adsorbents compared to CR. This is because the (π - π)-electron acceptor/donor interactions and H-bonding between adsorbent and dye were low when the pH of the solution was higher than the pK_a of the CR dye [48]. Moreover, the removal capacity of CR by PPSH and PPSOH decreased with increasing pH, and the better adsorption capacity occurred proximate of pH 2.0, with obvious differences.

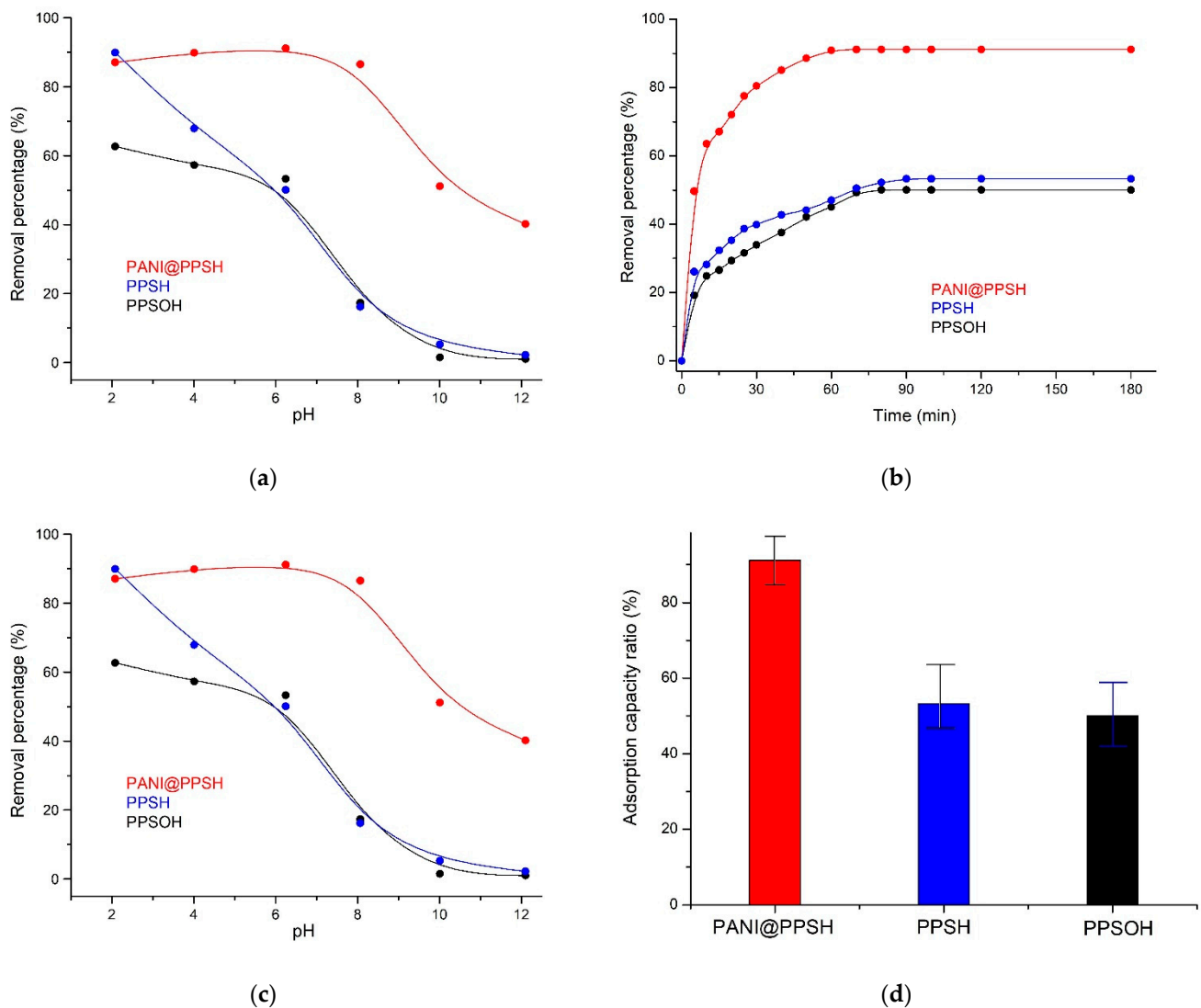


Figure 5. (a) Influence of pH on CR adsorption, (b) effect of contact time, (c) adsorption isotherm, and (d) comparison of adsorption efficiency of adsorbents (C_0 : $20 \text{ mg}\cdot\text{L}^{-1}$; adsorbents dose: 0.1 g ; CR: 100 mL ; T: 298 K ; pH = 6.5).

3.2.2. Contact Time Study

The influence of contact time on the elimination of CR dye by the three adsorbents prepared is depicted in Figure 5b. The initial concentrations of CR were $20 \text{ mg}\cdot\text{L}^{-1}$ at pH 6.5 and at ambient temperature. It was observed that the removal capacity of PANI@PPSH for CR dye increased rapidly when the contact time was increased between 0 and 50 min, which was related to the large surface area and large number of unoccupied adsorption sites

of this nanoadsorbent. The adsorption ratio became slower after 50 min, mainly due to the low dye concentration leading to a weaker elimination driving force in elimination, while the number active surface sites of nanoadsorbent also decreased. The removal capacity reached equilibrium after 60 min, and the elimination efficiency was 91.14%. Moreover, for the PPSH sample, the percentage of absorption required for CR to reach equilibrium decreased to 53.28%. This proved that the absorption of CR is related to the specific surface area, indicating the importance of the polymer matrix on the PPSH surface in accelerating the diffusion of the CR structure into the pores. In contrast, the PPSH required more than 70 min to adsorb only 51.66% of CR, while the PPSOH (50.06%) exhibited a somewhat repulsive interaction toward surface saturation at the end of the elimination process.

3.2.3. Adsorption Kinetics

Adsorption kinetics were explained and evaluated by using pseudo-first-order (PFO), pseudo-second-order (PSO), and intraparticle diffusion (the Weber–Morris) models.

The PFO kinetic describes the removal occurring between solid–liquid systems depending upon the removal capability of adsorbents [49]. The linear formula for PSO kinetic is equated as follows [50]:

$$\log(Q_e - Q_t) = \log Q_e - \frac{k_1}{2.303} t \quad (3)$$

where Q_e and Q_t are the equilibrium concentration and concentration at time t of CR ($\text{mg} \cdot \text{g}^{-1}$), respectively, and k_1 (min^{-1}) is the PFO rate constant. The PFO linear fitting plot of $\log(Q_{\text{eq}} - Q_i)$ versus t presents a poor correlation coefficient (Table 2), showing that the removal process did not follow the PFO kinetic model.

The PSO kinetic equation depicts a chemisorption phenomenon from solution [43], and it is obtained via the following formula [51]:

$$\frac{t}{Q_t} = \frac{1}{k_2 Q_e^2} + \frac{1}{Q_e} t \quad (4)$$

where k_2 ($\text{g} \cdot \text{mg}^{-1} \cdot \text{min}^{-1}$) is the PSO rate constant, Q_e and Q_t ($\text{mg} \cdot \text{g}^{-1}$) are the adsorption capacity at equilibrium and at time t , respectively, and $k_2 Q_e^2$ ($\text{g} \cdot \text{mg}^{-1} \cdot \text{min}$) represents the initial adsorption rate.

In order to identify more the kinetic mechanism of the adsorption process, intraparticle diffusion (the Weber–Morris) type was used to simulate the adsorption kinetics of CR on adsorbents as follows:

$$Q_t = k_i t^{0.5} + C \quad (5)$$

where Q_t is the adsorbed amount at time t ($\text{mg} \cdot \text{g}^{-1}$), C is the maximum adsorption amount, and k_i is the intraparticle diffusion rate constant ($\text{g} \cdot \text{mg}^{-1} \cdot \text{min}^{-1}$).

The PSO model fit the acquired data better than the PFO formula. Thus, the PSO equation was more efficient in defining the kinetics of the selected CR on these adsorbents and proved that the adsorption was chemisorption. The high correlation coefficients and adsorption rate of CR are given in Table 2. Moreover, the calculated value of $Q_{\text{eq,Cal}}$ obtained from the PSO form was close to the empirical values of $Q_{\text{eq,Exp}}$. On the other hand, the intraparticle diffusion model had a lower R^2 than the other two models. Moreover, the $C < 0$ was reported in previous removal studies and illustrated that external film diffusion limits the elimination rate in addition to intraparticle diffusion [52]. Therefore, the negative values of C can be interpreted as an external intraparticle diffusion resistance leading to the time delay in CR removal.

Table 2. PFO, PSO, and intraparticle diffusion sorption rate constants and Q_{eq} value for the elimination of CR on adsorbent samples at 298 K, pH: 6.5, and C_0 : 20 mg·L⁻¹.

Models	Constants	PPSH	PPSOH	PANI@PPSH
PFO	k_1 (min ⁻¹)	0.039	0.028	0.015
	$Q_{eq,Cal}$ (/mg·g ⁻¹)	10.06	10.67	3.87
	R^2	0.83	0.84	0.75
PSO	$k_{2,ads}$ (g·mg ⁻¹ ·min ⁻¹)	0.0160	0.0149	0.0103
	$Q_{eq,Cal}$ (mg·g ⁻¹)	9.71	8.18	17.88
	R^2	0.99	0.98	0.99
Intraparticle diffusion	k_i (g·mg ⁻¹ ·min ⁻¹)	0.227	0.225	0.121
	C (mg·g ⁻¹)	-1.72	-2.49	-2.52
	R^2	0.81	0.82	0.66

3.3. Adsorption Isotherms

Modeling the adsorption process is the key to revealing the adsorption mechanism. As illustrated in Figure 5c, the maximum adsorption capacity was explored and its adsorption behavior was determined through examining the isotherm adsorption models of CR onto adsorbents. The Freundlich, Langmuir, and Temkin models were selected to fit the empirical data.

The Langmuir model exhibited the adsorbents' surface to be uniform, consisting of fixed numbers of adsorption sites. Additionally, the removal was monolayer. The linear law is demonstrated as follows [53]:

$$\frac{C_{eq}}{Q_{eq}} = \frac{1}{K_l C_m} + \frac{C_{eq}}{Q_m} \quad (6)$$

where Q_{eq} (mg·g⁻¹), C_{eq} (mg·L⁻¹), and Q_m (mg·g⁻¹) represent the amount adsorbed, the equilibrium concentration of the adsorbate, and the monolayer adsorption capacity, respectively; K_l (L·mg⁻¹) represents the Langmuir constant.

Both multilayer (physisorption) and monolayer (chemisorption) can be measured using the Freundlich model. This form is depending on the heterogeneous equilibrium on adsorbents' surface. The Freundlich formula is presented as follows [50]:

$$\ln Q_{eq} = \ln K_f + \frac{1}{n} \ln C_{eq} \quad (7)$$

where K_f (mg⁻¹/n·L/n·g⁻¹) represents the Freundlich constant and $\frac{1}{n}$ symbolizes the Freundlich factor.

The Temkin model assumes a uniform distribution of binding energy up to a certain better level. It is based on the assumption that the heat of adsorption will not remain constant. It is expressed by Equations (8) and (9) [52]:

$$Q_{eq} = B \ln A_T + B \ln C_{eq} \quad (8)$$

$$B = \frac{RT}{b_T} \quad (9)$$

where b_T is the Temkin constant, A_T (L·g⁻¹) is the binding constant, R (8.314 J·mol⁻¹·K⁻¹) is the universal gas constant, B (J·mol⁻¹) is the constant related to the heat of sorption, and T (K) is Temperature.

The adsorption isotherms of the three adsorbents prepared are displayed in Figure 5c. The experimental values were successfully fitted to the Freundlich isotherm; this confirmed

the multilayer surface coverage [39]. The Freundlich isotherm parameters depicted maximum percentage removal efficiencies of 91.13%, 53.28%, and 50.06% for PANI@PPSH, PPSH, and PPSOH, respectively, and a like affinity to CR binding (Table 3). The formation of PPSH on the PANI matrix greatly increased the elimination capacity. This behavior was due to the large specific area provided by the polymer chain (such as aromatic units, amine, and imine functions) that produces novel active sites where CR could bind by electrostatics or π - π interactions [39,54]. Conversely, in the absence of PANI on the PPSH surface, the elimination capacity decreased because PPSH sites became saturated quickly due to the diminutive pores, and the effluent was not being treated completely [53]. In this way, a higher elimination capacity was obtained for the PANI@PPSH because of the formation of more active binding sites. This higher elimination was reflected in the adsorption efficacy since capacity higher than $17.14 \text{ mg}\cdot\text{g}^{-1}$ was obtained at weak concentrations and an adsorbent dosage of $20 \text{ mg}\cdot\text{L}^{-1}$. Moreover, values of correlation coefficient (R^2) found using the linear transformation of the Temkin model were comparable to the Freundlich isotherm. The variation of adsorption energy, b_T , was positive for all the studied adsorbents, implying that the adsorption of CR by this material is an exothermic reaction.

Table 3. Langmuir, Freundlich, and Temkin isotherms' data for CR removal by samples at 298 K and pH: 6.5.

Adsorbents	Constants	PPSH	PPSOH	PANI@PPSH
Langmuir	$Q_m \text{ (mg}\cdot\text{g}^{-1})$	21.83	13.57	27.10
	$K_L \text{ (L}\cdot\text{mg}^{-1})$	0.051	0.104	0.076
	R_L	0.474	0.415	0.327
	R^2	0.726	0.864	0.826
Freundlich	$K_F \text{ (mg}^{1-1/n}\text{L}^{1/n}\text{g}^{-1})$	0.925	1.290	1.716
	n	1.30	1.65	1.43
	R^2	0.977	0.917	0.930
Temkin	B	2.997	5.043	4.103
	$A_T \text{ (L}\cdot\text{g}^{-1})$	1.589	0.806	11.17
	$b_T \text{ (J}\cdot\text{mol}^{-1})$	826.57	491.24	603.79
	R^2	0.906	0.994	0.914

Figure 5d presents the comparison of elimination capacity of a hybrid adsorbent with PPSH and PPSOH. It was remarked that the CR adsorption capacity of PPSH was 1.7 times lower than that of the hybrid adsorbent, whereas PPSOH provided only 50.06% elimination capacity. These capacities were much lower than PANI@PPSH. The results confirmed that the existence of the PANI matrix in the hybrid adsorbent played a major role in CR elimination.

Polymers induced the generation of adsorption active sites for CR, which in turn increased removal capacity. On the other hand, a comparison of relative adsorption using different adsorbent materials based on the literature is summarized in Table 4 [55–71].

Table 4. Adsorption efficiencies (%) of Congo Red (CR) dye on several adsorbents.

Adsorbents	Adsorption Efficiency	pH	C_0 of CR (mg·L ⁻¹)	Ref.
Sawdust	31.2	7.0	20	[55]
Jujuba seeds	55.56	2.0	25	[56]
Activated red mud	7.08	7.0	//	[57]
Rubber seeds	9.82	6.0	//	[58]
Cashew nutshell	5.14	2.0	//	[59]
Pineapple plant stem	11.97	4.0	50	[60]

Table 4. Cont.

Adsorbents	Adsorption Efficiency	pH	C ₀ of CR (mg·L ⁻¹)	Ref.
Raw pinecone	10.28	5.8	//	[61]
Kenaf Self-activation	14.16	6.95	1000	[62]
Biochar	11.00	7.5	1000	[63]
FS@CS-PAA	19.72	5.0	50	[64]
TiO ₂ -NPs-ACWR	17.00	4.3	10	[65]
Apricot stone	23.42	13	100	[66]
Clay-biochar composite	11.9	5.7	20	[67]
Pine bark-derived char	3.92	7.0	5	[68]
Activated carbon (Coir pith)	6.72	6.3	40	[69]
Chitosan/Montmorillonite	12.70	3.0	200	[70]
Bengal gram fruit shell (SP)	22.22	6.95	50	[71]
PANI@PPSH	17.14	6.5	20	This work

3.4. Adsorption Thermodynamics

The entropy change (ΔS) and enthalpy content change (ΔH) were determined by the van't Hoff law:

$$\ln\left(\frac{Q_{\text{eq}}}{C_{\text{eq}}}\right) = -\frac{\Delta H}{RT} + \frac{\Delta S}{R} \quad (10)$$

The Gibbs free energy (ΔG) can be measured via the following law:

$$\Delta G = \Delta H - T\Delta S \quad (11)$$

where R ($8.314 \text{ J}\cdot\text{mol}^{-1}\cdot\text{K}^{-1}$) represents the general gas constant and T (K) represents the absolute temperature.

Because of the influence of temperature on the CR removal by adsorbents, the thermodynamic data of PPSH, PPSOH, and PANI@PPSH were investigated at distinct temperatures (Figure 6a). The ΔS and ΔH values were calculated using the slope and intercept according to the van't Hoff equation [72]. For PANI@PPSH and PPSH, the ΔG was negative (Table 5), suggesting that the process was workable and adsorption was spontaneous thermodynamically, while the positive ΔG values of PPSOH proved that it was thermodynamically unfavorable for efficient elimination, with like results reported in the literature [73]. At the same time, the positive value of ΔH proved that the interaction between the CR dye and adsorbents was exothermic processes [74]. Besides, the adsorption process might be chemical or physical. Participating force links in the physical removal operation were feeble. Thus, the heat of elimination generally was less than $21 \text{ kJ}\cdot\text{mol}^{-1}$. In physical elimination, involved force links are less powerful than chemical removal and the heat of elimination in chemical adsorption is such that the heat of the chemical reaction is around 21 to $42 \text{ kJ}\cdot\text{mol}^{-1}$ [75]. In this way, the achieved ΔH value ($20.75 \text{ kJ}\cdot\text{mol}^{-1}$) and the elimination of CR by PANI@PPSH adsorbent was physical adsorption. The positive ΔS value indicated that the density of the system increased with the adsorption of CR on the adsorbent samples.

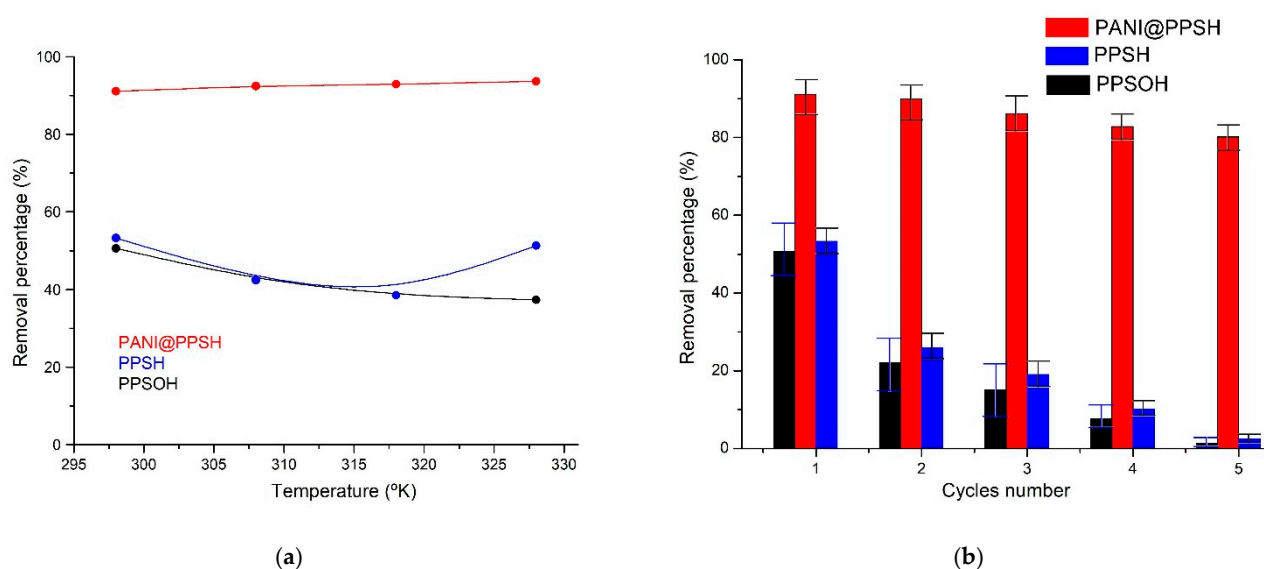


Figure 6. (a) Influence of temperature on elimination percentage and (b) cyclic adsorption–desorption performance of adsorbents on CR (C_0 : $20 \text{ mg}\cdot\text{L}^{-1}$; adsorbents dose: 0.1 g ; CR: 100 mL ; T: 298 K ; pH 6.5).

Table 5. Thermodynamic data for CR adsorption by the three adsorbents prepared.

Adsorbents	T (K)	$\Delta G \text{ (kJ}\cdot\text{mol}^{-1})$	$\Delta H \text{ (kJ}\cdot\text{mol}^{-1})$	$\Delta S \text{ (kJ}\cdot\text{mol}^{-1})$
PPSH	298	−0.30	23.54	0.080
	308	−1.10		
	318	−1.90		
	328	−2.70		
PPSOH	298	1.012	10.25	0.031
	308	0.702		
	318	0.392		
	328	0.082		
PANI@PPSH	298	−4.878	20.75	0.086
	308	−5.738		
	318	−6.598		
	328	−7.458		

3.5. Adsorption Mechanism

The mechanism of dye removal through the adsorbents in aqueous solution can be influenced by many factors, including the surface area of adsorbents, the textural properties, and the nature of the interaction between the adsorbents and the dyes, such as π – π stacking, hydrogen bonding, electrostatic attractions, ion exchange, coordination, and acid/base interaction [76]. Moreover, based on the above analyses of the isothermal and kinetic models, physisorption (multilayer) and chemisorption (monolayer) adsorption probably dominate the adsorption process on a uniform surface. Furthermore, the existence of the PANI chain on the PPSH surface caused the surface to be negatively charged, which played an important role in these elimination processes. The adsorption mechanisms can be illustrated in two formats. Physisorption can be realized on the PANI structure surface or/and into PPSH porosity, or chemisorption by interaction between CR dye and PANI backbone. In addition, there is a possibility of hydrogen bonding between amine functions of polymer and nitrogen existing in the CR structure. Furthermore, the existence of benzene

and quinone units with a delocalized π -conjugated structure and electrochemically active sites in the polymer chain creates an additional factor into the PPSH surface and ameliorates the favorable adsorption of CR dye. Accordingly, the IR spectrum for PANI@PPSH was obtained after CR adsorption (Figure 1b), indicating the effect of CR adsorption by different functional groups (the changes in the wavenumber, reduction, and disappearance of the bands were evident according to the IR spectrum peaks). These results are consistent with the studies of Chan et al. [60], which suggested a formation of a binding of CR to different functional groups on the surface of the adsorbent.

3.6. Stability and Recyclability of Adsorbents

The regenerability of the material is an important parameter to evaluate whether the adsorbent can be used in practice. The response surface optimized conditions of pH 6.5 and 1 g/L of 20 mg·L⁻¹ CR concentration, followed by elution with C₂H₅OH, H₃PO₄ (1 M), and finally by distilled water. Five consecutive adsorption/desorption tests were performed to evaluate the reusability of the adsorbent samples. The elimination rates obtained are shown in Figure 6b. After five experiments, PANI@PPSH still showed a good regeneration rate and the removal rate at a high 80%, whereas the adsorption capacity of PPSH and PPSOH decreased to 2.43% and 1.28% after five cycles, respectively. This showed that desorption in the acid solution helped to restore the pristine structure of PANI (Emeraldine salt), which was the main compound in the hybrid adsorbent [77]. In the existence of acid, the amine nitrogen atoms of CR tend to evolve a positive charge. In contrast, the electrostatic attractive forces between the CR dye and the hybrid adsorbent can be weakened, leading to desorption of CR from PANI@PPSH.

4. Conclusions

A novel, activated carbon (PPSH and PPSOH) was prepared by chemical activation of PPS with phosphoric acid and sodium hydroxide. PANI chains were grown on the surface of the PPSH support by in situ polymerization to significantly improve the CR removal capacity. The characterization of the obtained adsorbents was performed by XRD, XPS, FTIR, SEM, TGA, and N₂ adsorption/desorption isotherms. Using PANI@PPSH as adsorbent, the maximum adsorption capacity for CR dye reached 17.14 mg·g⁻¹, and the obtained results proved that the PSO model fit the experimental values well. Moreover, the Freundlich and Temkin isotherm models were found to be much better than the Langmuir isotherm model in describing the removal behavior of the dye by the hybrid adsorbent, indicating that the active sites were saturated and a chemical adsorption mechanism was present. Significantly, the hybrid adsorbent exhibited the highest adsorption capacity (80.15%) after five cycles of the adsorption/desorption process. These results indicate that, in general, the PANI matrix can be better used for elimination when it is distributed on the surface of suitable support materials. In addition, thermodynamic studies indicate that the adsorption process is exothermic and spontaneous.

Author Contributions: Conceptualization, S.L. and A.B.; methodology: L.S. and A.B.; software: I.M. and A.B.; validation: L.S. and A.B.; formal analysis: S.L., A.E.K. and A.B.; investigation: S.L., I.M., A.E.K. and A.B.; data curation: S.L., I.M., M.K. and A.B.; writing—original draft preparation, S.L. and L.S.; writing—review and editing, all authors; visualization, S.L., I.M., L.S. and A.B.; supervision, A.B. All authors have read and agreed to the published version of the manuscript.

Funding: This research received no external funding.

Data Availability Statement: All data created in this study are presented in this paper.

Acknowledgments: The authors thank the Algerian MESRS & DGRSDT and IUMA of Alicante University, Spain, for their collaboration.

Conflicts of Interest: The authors declare no conflict of interest.

References

1. Vallinayagam, S.; Rajendran, K.; Lakkaboyana, S.K.; Soontarapa, K.; Remya, R.R.; Sharma, V.K.; Kumar, V.; Venkateswarlu, K.; Koduru, J.R. Recent developments in magnetic nanoparticles and nano-composites for wastewater treatment. *J. Environ. Chem. Eng.* **2021**, *9*, 106553. [[CrossRef](#)]
2. Wang, S.; Zhang, B.; Shan, C.; Yan, X.; Chen, H.; Pan, B. Occurrence and transformation of phosphonates in textile dyeing wastewater along full-scale combined treatment processes. *Water Res.* **2020**, *184*, 116173. [[CrossRef](#)] [[PubMed](#)]
3. Prasannan, A.; Udomsin, J.; Tsai, H.-C.; Sivakumar, M.; Hu, C.-C.; Wang, C.-F.; Hung, W.-S.; Lai, J.-Y. Special wettable underwater superoleophobic material for effective simultaneous removal of high viscous insoluble oils and soluble dyes from wastewater. *J. Memb. Sci.* **2020**, *603*, 118026. [[CrossRef](#)]
4. Solangi, N.H.; Kumar, J.; Mazari, S.A.; Ahmed, S.; Fatima, N.; Mubarak, N.M. Development of fruit waste derived bio-adsorbents for wastewater treatment: A review. *J. Hazard. Mater.* **2021**, *416*, 125848. [[CrossRef](#)]
5. Yang, L.; Zhan, Y.; Yu, R.; Lan, J.; Shang, J.; Dou, B.; Liu, H.; Zou, R.; Lin, S. Facile and scalable fabrication of antibacterial CO₂-Responsive cotton for ultrafast and controllable removal of anionic dyes. *ACS Appl. Mater. Interfaces* **2021**, *13*, 2694–2709. [[CrossRef](#)]
6. Malik, A.; Nath, M. Synthesis of Ag/ZIF-7 by immobilization of Ag nanoparticles onto ZIF-7 microcrystals: A heterogeneous catalyst for the reduction of nitroaromatic compounds and organic dyes. *J. Environ. Chem. Eng.* **2020**, *8*, 104547. [[CrossRef](#)]
7. Gao, Y.; Yan, S.; He, Y.; Fan, Y.J.; Zhang, L.; Ma, J.; Hou, R.; Chen, L.; Chen, J. A photo-Fenton self-cleaning membrane based on NH₂-MIL-88B (Fe) and graphene oxide to improve dye removal performance. *J. Memb. Sci.* **2021**, *626*, 119192. [[CrossRef](#)]
8. Yang, Y.; Xiong, Z.; Wang, Z.; Liu, Y.; He, Z.; Cao, A.; Zhou, L.; Zhu, L.; Zhao, S. Super-adsorptive and photo-regenerable carbon nanotube based membrane for highly efficient water purification. *J. Memb. Sci.* **2021**, *621*, 119000. [[CrossRef](#)]
9. Zhou, S.; Feng, X.; Zhu, J.; Song, Q.; Yang, G.; Zhang, Y.; Van der Bruggen, B. Self-cleaning loose nanofiltration membranes enabled by photocatalytic Cu-triazolate MOFs for dye/salt separation. *J. Memb. Sci.* **2021**, *623*, 119058. [[CrossRef](#)]
10. Lakkaboyana, S.K.; Soontarapa, K.; Kumar, V.; Marella, R.K.; Kannan, K. Preparation of novel chitosan polymeric nanocomposite as an efficient material for the removal of Acid Blue 25 from aqueous environment. *Int. J. Biol. Macromol.* **2021**, *168*, 760–768. [[CrossRef](#)] [[PubMed](#)]
11. Liang, H.; Sun, R.; Song, B.; Sun, Q.; Peng, P.; She, D. Preparation of nitrogen-doped porous carbon material by a hydrothermal-activation two-step method and its high-efficiency adsorption of Cr(VI). *J. Hazard. Mater.* **2020**, *387*, 121987. [[CrossRef](#)] [[PubMed](#)]
12. Wu, X.Q.; Huang, D.D.; Wu, Y.P.; Zhao, J.; Liu, X.; Dong, W.W.; Li, S.; Li, D.S.; Li, J.R. In Situ Synthesis of Nano CuS-Embedded MOF Hierarchical Structures and Application in Dye Adsorption and Hydrogen Evolution Reaction. *ACS Appl. Energy Mater.* **2019**, *2*, 5698–5706. [[CrossRef](#)]
13. Deng, J.; Chen, L.; Hong, S.; Lian, H. UZnCl₂-DES assisted synthesis of phenolic resin-based carbon aerogels for capacitors. *J. Porous Mater.* **2020**, *27*, 789–800. [[CrossRef](#)]
14. Diez, N.; Ferrero, G.A.; Sevilla, M.; Fuertes, A.B. A sustainable approach to hierarchically porous carbons from tannic acid and their utilization in supercapacitive energy storage systems. *J. Mater. Chem. A* **2019**, *7*, 14280–14290. [[CrossRef](#)]
15. Tong, S.; Sun, Y.; Li, X.; Hu, Z.; Worasuwannarak, N.; Liu, H.; Hu, H.; Luo, G.; Yao, H. Gas-pressurized torrefaction of biomass wastes: Co-gasification of gas-pressurized torrefied biomass with coal. *Bioresour. Technol.* **2020**, *321*, 124505. [[CrossRef](#)] [[PubMed](#)]
16. Waribam, P.; Ngo, S.D.; Tran, T.T.V.; Kongparakul, S.; Reubroycharoen, P.; Chanlek, N.; Wei, L.; Zhang, H.; Guan, G.; Samart, C. Waste biomass valorization through production of xylose-based porous carbon microspheres for supercapacitor applications. *Waste Manag.* **2020**, *105*, 492–500. [[CrossRef](#)] [[PubMed](#)]
17. Choi, S.W.; Tang, J.; Pol, V.G.; Lee, K.B. Pollen-derived porous carbon by KOH activation: Effect of physicochemical structure on CO₂ adsorption. *J. CO₂ Util.* **2019**, *29*, 146–155. [[CrossRef](#)]
18. Dai, C.; Wan, J.; Yang, J.; Qu, S.; Jin, T.; Ma, F.; Shao, J. H₃PO₄ solution hydrothermal carbonization combined with KOH activation to prepare argy wormwood-based porous carbon for high-performance supercapacitors. *Appl. Surf. Sci.* **2018**, *444*, 105–117. [[CrossRef](#)]
19. Xue, H.; Wang, X.; Xu, Q.; Dhaouadi, F.; Sellaoui, B.; Seliem, M.K.; Lamine, A.B.; Belmabrouk, H.; Bajahzar, A.; Petriciolet, A.B.; et al. Adsorption of methylene blue from aqueous solution on activated carbons and composite prepared from an agricultural waste biomass: A comparative study by experimental and advanced modeling analysis. *Chem. Eng. J.* **2022**, *430*, 132801. [[CrossRef](#)]
20. Pang, X.; Sellaoui, L.; Franco, D.; Netto, M.S.; Georgin, J.; Dotto, G.L.; Shayeb, M.K.A.; Belmabrouk, H.; Petriciolet, A.B.; Li, Z. Preparation and characterization of a novel mountain soursop seeds powder adsorbent and its application for the removal of crystal violet and methylene blue from aqueous solutions. *Chem. Eng. J.* **2020**, *391*, 123617. [[CrossRef](#)]
21. Pang, X.; Sellaoui, L.; Franco, D.; Dotto, G.L.; Georgin, J.; Bajahzar, A.; Belmabrouk, H.; Lamine, A.B.; Petriciolet, A.B.; Li, Z. Adsorption of crystal violet on biomasses from pecan nutshell, para chestnut husk, araucaria bark and palm cactus: Experimental study and theoretical modeling via monolayer and double layer statistical physics models. *Chem. Eng. J.* **2019**, *378*, 122101. [[CrossRef](#)]
22. Amran, F.; Zaini, M.A.A. Valorization of Casuarina empty fruit-based activated carbons for dyes removal—Activators, isotherm, kinetics and thermodynamics. *Surf. Interfaces* **2021**, *25*, 101277. [[CrossRef](#)]
23. Chakraborty, S.; Farida, J.J.; Simon, R.; Kasthuri, S.; Mary, N.L. Averrhoë carrambola fruit extract assisted green synthesis of ZnO nanoparticles for the photodegradation of Congo red dye. *Surf. Interfaces* **2020**, *19*, 100488. [[CrossRef](#)]

24. Guerrero-Beltrán, J.Á.; Ochoa-Velasco, C.E. Figo da india—Opuntia spp. In *Exotic Fruits*; Rodrigues, S., de Oliveira Silva, E., de Brito, E.S.B.T.-E.F., Eds.; Academic Press: Cambridge, MA, USA, 2018; pp. 187–201. ISBN 978-0-12-803138-4.
25. Piga, A.G. Cactus pear: A fruit of nutraceutical and functional importance. *J. Prof. Assoc. Cactus Dev.* **2004**, *6*, 9–22.
26. Al Juhaimi, F.; Ghafoor, K.; Uslu, N.; Mohamed Ahmed, I.A.; Babiker, E.E.; Özcan, M.M.; Fadimu, G.J. The effect of harvest times on bioactive properties and fatty acid compositions of prickly pear (*Opuntia ficus-barbarica* A. Berger) fruits. *Food Chem.* **2020**, *303*, 125387. [[CrossRef](#)] [[PubMed](#)]
27. Saenz, C. Processing technologies: An alternative for cactus pear (*Opuntia* spp.) fruits and cladodes. *J. Arid. Environ.* **2000**, *46*, 209–225. [[CrossRef](#)]
28. Özcan, M.M.; Al Juhaimi, F.Y. Nutritive value and chemical composition of prickly pear seeds (*Opuntia ficus indica* L.) growing in Turkey. *Int. J. Food Sci. Nutr.* **2011**, *62*, 533–536. [[CrossRef](#)]
29. Barka, N.; Abdennouri, M.; El Makhfouk, M.; Qourzal, S. Biosorption characteristics of cadmium and lead onto eco-friendly dried cactus (*Opuntia ficus indica*) cladodes. *J. Environ. Chem. Eng.* **2013**, *1*, 144–149. [[CrossRef](#)]
30. Peláez-Cid, A.A.; Velázquez-Ugalde, I.; Herrera-González, A.M.; García-Serrano, J. Textile dyes removal from aqueous solution using *Opuntia ficus-indica* fruit waste as adsorbent and its characterization. *J. Environ. Manag.* **2013**, *130*, 90–97. [[CrossRef](#)]
31. Bekhoukh, A.; Moulefera, I.; Zeggai, F.Z.; Benyoucef, A.; Bachari, K. Anionic Methyl Orange Removal from Aqueous Solutions by Activated Carbon Reinforced Conducting Polyaniline as Adsorbent: Synthesis, Characterization, Adsorption Behavior, Regeneration and Kinetics Study. Available online: <https://link.springer.com/article/10.1007/s10924-021-02248-6> (accessed on 30 October 2021).
32. Mahi, O.; Khaldi, K.; Belardja, M.S.; Belmokhtar, A.; Benyoucef, A. Development of a New Hybrid Adsorbent from *Opuntia ficus indica* NaOH-Activated with PANI-Reinforced and Its Potential Use in Orange-G Dye Removal. *J. Inorg. Organomet. Polym. Mater.* **2021**, *31*, 2095–2104. [[CrossRef](#)]
33. Bekhti, M.; Belardja, M.S.; Lafjah, M.; Chouli, F.; Benyoucef, A. Enhanced tailored of thermal stability, optical and electrochemical properties of PANI matrix containing Al₂O₃ hybrid materials synthesized through in situ polymerization. *Polym. Compos.* **2020**, *42*, 6–14. [[CrossRef](#)]
34. Nepomuceno, N.C.; Seixas, A.A.A.; Medeiros, E.S.; Mélo, T.J.A. Evaluation of conductivity of nanostructured polyaniline/cellulose nanocrystals (PANI/CNC) obtained via in situ polymerization. *J. Solid State Chem.* **2021**, *302*, 122372. [[CrossRef](#)]
35. Hsini, A.; Naciri, Y.; Laabd, M.; El Ouardi, M.; Ajmal, Z.; Lakhmiri, R.; Boukherroub, R.; Albourine, A. Synthesis and characterization of arginine-doped polyaniline/walnut shell hybrid composite with superior clean-up ability for chromium (VI) from aqueous media: Equilibrium, reusability and process optimization. *J. Mol. Liq.* **2020**, *316*, 113832. [[CrossRef](#)]
36. Hsini, A.; Essekre, A.; Aarab, N.; Laabd, M.; Ait Addi, A.; Lakhmiri, R.; Albourine, A. Elaboration of novel polyaniline@Almond shell biocomposite for effective removal of hexavalent chromium ions and Orange G dye from aqueous solutions. *Environ. Sci. Pollut. Res.* **2020**, *27*, 15245–15258. [[CrossRef](#)]
37. Sahnoun, S.; Boutahala, M. Adsorption removal of tartrazine by chitosan/polyaniline composite: Kinetics and equilibrium studies. *Int. J. Biol. Macromol.* **2018**, *114*, 1345–1353. [[CrossRef](#)] [[PubMed](#)]
38. Imgharn, A.; Ighnih, H.; Hsini, A.; Naciri, Y.; Laabd, M.; Kabli, H.; Elamine, M.; Lakhmiri, R.; Souhail, B.; Albourine, A. Synthesis and characterization of polyaniline-based biocomposites and their application for effective removal of Orange G dye using adsorption in dynamic regime. *Chem. Phys. Lett.* **2021**, *778*, 138811. [[CrossRef](#)]
39. Toumi, I.; Djelad, H.; Chouli, F.; Benyoucef, A. Synthesis of PANI@ZnO Hybrid Material and Evaluations in Adsorption of Congo Red and Methylene Blue Dyes: Structural Characterization and Adsorption Performance. *J. Inorg. Organomet. Polym. Mater.* **2021**, *32*, 112–121. [[CrossRef](#)]
40. Belhajjia, C.; Abid, A.; Msaad, A.; Labaali, Z.; Zouhri, A. Synthesis, characterization and adsorption of Malachite green dye using novel materiel produced from *Opuntia ficus indica*. *Mater. Today Proc.* **2021**, *37*, 4001–4006. [[CrossRef](#)]
41. Bhattacharyya, R.; Ray, S.K. Adsorption of industrial dyes by semi-IPN hydrogels of Acrylic copolymers and sodium alginate. *J. Ind. Eng. Chem.* **2015**, *22*, 92–102. [[CrossRef](#)]
42. Mannai, F.; Elhleli, H.; Ammar, M.; Passas, R.; Elaloui, E.; Moussaoui, Y. Green process for fibrous networks extraction from *Opuntia* (Cactaceae): Morphological design, thermal and mechanical studies. *Ind. Crops Prod.* **2018**, *126*, 347–356. [[CrossRef](#)]
43. Pouget, J.P.; Jozefowicz, M.E.; Epstein, A.J.; Tang, X.; MacDiarmid, A.G. X-ray structure of polyaniline. *Macromolecules* **1991**, *24*, 779–789. [[CrossRef](#)]
44. Gupta, S.P.; Nishad, H.H.; Chakane, S.D.; Gosavi, S.W.; Late, D.J.; Walke, P.S. Phase transformation in tungsten oxide nanoplates as a function of post-annealing temperature and its electrochemical influence on energy storage. *Nanoscale Adv.* **2020**, *2*, 4689–4701. [[CrossRef](#)]
45. Kuzmenko, V.; Wang, N.; Haque, M.; Naboka, O.; Flygare, M.; Svensson, K.; Gatenholm, P.; Liu, J.; Enoksson, P. Cellulose-derived carbon nanofibers/graphene composite electrodes for powerful compact supercapacitors. *RSC Adv.* **2017**, *7*, 45968–45977. [[CrossRef](#)]
46. Jiao, C.; Zhang, Z.; Tao, J.; Zhang, D.; Chen, Y.; Lin, H. Synthesis of a poly(amidoxime-hydroxamic acid) cellulose derivative and its application in heavy metal ion removal. *RSC Adv.* **2017**, *7*, 27787–27795. [[CrossRef](#)]
47. Habibi, M.K.; Rafiaei, S.M.; Alhaji, A.; Zare, M. Synthesis of ZnFe₂O₄: 1 wt% Ce³⁺/Carbon fibers composite and investigation of its adsorption characteristic to remove Congo red dye from aqueous solutions. *J. Alloys Compd.* **2022**, *890*, 161901. [[CrossRef](#)]

48. Ahmed, M.B.; Zhou, J.L.; Ngo, H.H.; Johir, A.H.; Sornalingam, K. Sorptive removal of phenolic endocrine disruptors by functionalized biochar: Competitive interaction mechanism, removal efficacy and application in wastewater. *Chem. Eng. J.* **2018**, *335*, 801–811. [[CrossRef](#)]
49. Yuh-Shan, H. Citation review of Lagergren kinetic rate equation on adsorption reactions. *Scientometrics* **2004**, *59*, 171–177. [[CrossRef](#)]
50. Lagergren, S. Zur Theorie der sogenannten Adsorption gelöster Stoffe. *Z. Chem. Ind. Kolloide* **1898**, *2*, 4.
51. Azizian, S. Kinetic models of sorption: A theoretical analysis. *J. Colloid Interface Sci.* **2004**, *276*, 47–52. [[CrossRef](#)]
52. Duan, R.; Fedler, C.B.; Jiao, X. Adsorption of pyridine from aqueous solutions onto polyaluminium chloride and anionic polyacrylamide water treatment residuals. *Water. Sci. Technol.* **2021**, *83*, 1753–1763. [[CrossRef](#)] [[PubMed](#)]
53. Ansari, M.O.; Kumar, R.; Ansari, S.A.; Ansari, S.P.; Barakat, M.A.; Alshahrie, A.; Cho, M.H. Anion selective pTSA doped polyaniline@graphene oxide-multiwalled carbon nanotube composite for Cr(VI) and Congo red adsorption. *J. Colloid Interface Sci.* **2017**, *496*, 407–415. [[CrossRef](#)]
54. González-López, M.E.; Laureano-Anzaldo, C.M.; Pérez-Fonseca, A.A.; Gómez, C.; Robledo-Ortíz, J.R. Congo red adsorption with cellulose-graphene nanoplatelets beads by differential column batch reactor. *J. Environ. Chem. Eng.* **2021**, *9*, 105029. [[CrossRef](#)]
55. Mane, V.S.; Vijay Babu, P.V. Kinetic and equilibrium studies on the removal of Congo red from aqueous solution using Eucalyptus wood (Eucalyptus globulus) saw dust. *J. Taiwan Inst. Chem. Eng.* **2013**, *44*, 81–88. [[CrossRef](#)]
56. Somasekhara Reddy, M.C.; Sivaramakrishna, L.; Varada Reddy, A. The use of an agricultural waste material, Jujuba seeds for the removal of anionic dye (Congo red) from aqueous medium. *J. Hazard. Mater.* **2012**, *203*, 118–127. [[CrossRef](#)]
57. Tor, A.; Cengeloglu, Y. Removal of congo red from aqueous solution by adsorption onto acid activated red mud. *J. Hazard. Mater.* **2006**, *138*, 409–415. [[CrossRef](#)] [[PubMed](#)]
58. Zulfikar, M.A.; Setiyanto, H.; Rusnadi; Solakhudin, L. Rubber seeds (Hevea brasiliensis): An adsorbent for adsorption of Congo red from aqueous solution. *Desalin. Water Treat.* **2014**, *56*, 2976–2987. [[CrossRef](#)]
59. Senthil Kumar, P.; Ramalingam, S.; Senthamarai, C.; Niranjanaa, M.; Vijayalakshmi, P.; Sivanesan, S. Adsorption of dye from aqueous solution by cashew nut shell: Studies on equilibrium isotherm, kinetics and thermodynamics of interactions. *Desalination* **2010**, *261*, 52–60. [[CrossRef](#)]
60. Chan, S.-L.; Tan, Y.P.; Abdullah, A.H.; Ong, S.-T. Equilibrium, kinetic and thermodynamic studies of a new potential biosorbent for the removal of Basic Blue 3 and Congo Red dyes: Pineapple (Ananas comosus) plant stem. *J. Taiwan Inst. Chem. Eng.* **2016**, *61*, 306–315. [[CrossRef](#)]
61. Dawood, S.; Sen, T.K. Removal of anionic dye Congo red from aqueous solution by raw pine and acid-treated pine cone powder as adsorbent: Equilibrium, thermodynamic, kinetics, mechanism and process design. *Water Res.* **2012**, *46*, 1933–1946. [[CrossRef](#)] [[PubMed](#)]
62. Mandal, S.; Calderon, J.; Marpu, S.B.; Omary, M.A.; Shi, S.Q. Mesoporous activated carbon as a green adsorbent for the removal of heavy metals and Congo red: Characterization, adsorption kinetics, and isotherm studies. *J. Contam. Hydrol.* **2021**, *243*, 103869. [[CrossRef](#)] [[PubMed](#)]
63. Yang, G.; Wu, L.; Xian, Q.; Shen, F.; Wu, J.; Zhang, Y. Removal of Congo red and methylene blue from aqueous solutions by vermicompost-derived biochars. *PLoS ONE* **2016**, *11*, e0154562. [[CrossRef](#)] [[PubMed](#)]
64. Zheng, X.; Zheng, H.; Xiong, Z.; Zhao, R.; Liu, Y.; Zhao, C.; Zheng, C. Novel anionic polyacrylamide-modify-chitosan magnetic composite nanoparticles with excellent adsorption capacity for cationic dyes and pH-independent adsorption capability for metal ions. *Chem. Eng. J.* **2020**, *392*, 123706. [[CrossRef](#)]
65. Masoudian, N.; Rajabi, M.; Ghaedi, M. Titanium oxide nanoparticles loaded onto activated carbon prepared from bio-waste watermelon rind for the efficient ultrasonic-assisted adsorption of congo red and phenol red dyes from wastewaters. *Polyhedron* **2019**, *173*, 114105. [[CrossRef](#)]
66. Abbas, M.; Trari, M. Kinetic, equilibrium and thermodynamic study on the removal of Congo Red from aqueous solutions by adsorption onto apricot stone. *Process Saf. Environ. Prot.* **2015**, *98*, 424–436. [[CrossRef](#)]
67. Yao, Y.; Gao, B.; Fang, J.; Zhang, M.; Chen, H.; Zhou, Y.; Creamer, A.E.; Sun, Y.; Yang, L. Characterization and environmental applications of clay–biochar composites. *Chem. Eng. J.* **2014**, *242*, 136–143. [[CrossRef](#)]
68. Litefti, K.; Freire, M.S.; Stitou, M.; González-Álvarez, J. Adsorption of an anionic dye (Congo red) from aqueous solutions by pine bark. *Sci. Rep.* **2019**, *9*, 16530. [[CrossRef](#)]
69. Namasivayam, C.; Kavitha, D. Removal of Congo Red from water by adsorption onto activated carbon prepared from coir pith, an agricultural solid waste. *Dye. Pigment.* **2002**, *54*, 47–58. [[CrossRef](#)]
70. Wang, L.; Wang, A. Adsorption characteristics of Congo Red onto the chitosan/montmorillonite nanocomposite. *J. Hazard. Mater.* **2007**, *147*, 979–985. [[CrossRef](#)]
71. Krishna, L.S.; Reddy, A.S.; Muralikrishna, A.; Zuhairi, W.Y.W.; Osman, H.; Reddy, A.V. Utilization of the agricultural waste (Cicer arietinum Linn fruit shell biomass) as biosorbent for decolorization of Congo red. *Desalin. Water Treat.* **2015**, *56*, 2181–2192. [[CrossRef](#)]
72. Moreno-López, J.C.; Pérez Paz, A.; Gottardi, S.; Solianyik, L.; Li, J.; Monjas, L.; Hirsch, A.K.H.; Mowbray, D.J.; Stöhr, M. Unveiling Adatoms in On-Surface Reactions: Combining Scanning Probe Microscopy with van't Hoff Plots. *J. Phys. Chem. C* **2021**, *125*, 9847–9854. [[CrossRef](#)]

73. Tay, S.Y.; Wong, V.L.; Lim, S.S.; Teo, I.L.R. Adsorption equilibrium, kinetics and thermodynamics studies of anionic methyl orange dye adsorption using chitosan-calcium chloride gel beads. *Chem. Eng. Commun.* **2021**, *208*, 708–726. [[CrossRef](#)]
74. Mydul Islam, A.K.M.; Hwang, J.I.; Lee, S.E.; Kim, J.E. Comparative study of carbon black and activated carbon adsorbents for removal of carbofuran from aqueous solution. *Desalin. Water Treat.* **2016**, *57*, 21512–21523. [[CrossRef](#)]
75. Shabandokht, M.; Binaeian, E.; Tayebi, H. Adsorption of food dye Acid red 18 onto polyaniline-modified rice husk composite: Isotherm and kinetic analysis. *Desalin. Water Treat.* **2016**, *57*, 27638–27650. [[CrossRef](#)]
76. Karami, K.; Beram, S.M.; Bayat, P.; Siadatnasab, F.; Ramezani, A. A novel nanohybrid based on metal-organic framework MIL101 -Cr/PANI/Ag for the adsorption of cationic methylene blue dye from aqueous solution. *J. Mol. Struct.* **2022**, *1247*, 131352. [[CrossRef](#)]
77. Pete, S.; Kattil, R.A.; Thomas, L. Polyaniline-multiwalled carbon nanotubes (PANI-MWCNTs) composite revisited: An efficient and reusable material for methyl orange dye removal. *Diam. Relat. Mater.* **2021**, *117*, 108455. [[CrossRef](#)]